First-principles calculations on bcc-hcp transition of titanium ⋆

Shigeto R. Nishitani [1]

Department of Materials Science and Engineering, Kyoto University, Kyoto 606–8501, Japan

Hitoshi Kawabe and Masato Aoki

Department of Electrical and Electronic Engineering, Gifu University, Gifu 501–1193, Japan

Abstract

Bcc-hcp transition of Ti was investigated by the first principles calculations. Very accurate calculations using the gradient-corrected FP-LMTO correctly estimated the hcp structure slightly lower in energy than the ω structure. The adiabatic potential energy surfaces of the distortions related to the structural transformations showed similar with those of Zr. The curvatures of the potential surfaces at the equilibrium bcc point are very small and negative, which suggests that Ti has strong anisotropic characters of bondings. The electronic thermal contribution stabilizes the bcc structure over the hcp structure above 3000K.

Key words: Ti, bcc-hcp allotropic transformation, FP-LMTO, phonon, finite temperature effect

1 Introduction

Bcc-hcp transition is one of the most frequently observed structural changes in martensitic transformation. It occurs not only in shape memory alloys but also in pure elements such as Ti and Zr. Experimentally, Petry and co-workers [1–3] studied the origin of the stability of the bcc structure in Ti, Zr and Hf metals by measurements of phonons at high temperatures, and they concluded that the

⋆ Accepted for publication in Matererials Science and Engineering A.

[1] E-mail:bob@karma.mtl.kyoto-u.ac.jp

increased entropy due to the low lying $T_1[\xi\xi 2\xi]$ and $T_1[\xi\xi 0]$ phonon branches plays a main role.

There are a number of researches on the electronic structure of Zr by the first principles calculations [4], lattice dynamics using empirical many body potentials [5–8], and realistic microstructural evaluations by molecular dynamic simulations [9]. All the calculations qualitatively show a consistent view on the relations of vibrational and electronic contributions, and are also consistent with the experimental data [2].

In contrast with the case of Zr, the first principles calculations on Ti are ambiguous. The main difficulty in the energy calculations for Ti comes from their accuracy, where the ω phase is incorrectly estimated to be more stable than the hcp structure [10,11].

Very recently, accurate calculations on Ti were performed by the authors [12] using full-potential linear muffin-tin orbitals (FP-LMTO) [13,14]. In this paper, we first summarize the current theoretical understanding on the bcc-hcp transition of Zr and Ti. Then we will show our results of first principles calculations on Ti. We will clarify the bonding characters of bcc Ti at the ground state and the electronic contributions to the stability of the bcc structure at high temperatures.

2 Phonon effects on bcc stability

In 1947 Zener [15] proposed a soft-mode model for the bcc-hcp transition, where the shear modulus $C' = \frac{1}{2}(C_{11} - C_{12})$ of the bcc structure approaches zero at the transition temperature. A similar model by Friedel concentrates on a particular short-wavelength phonon becoming unstable [16]. About a decade ago, Petry and co-workers [1–3] measured phonons in group-IV transition metals at the high temperatures where the bcc phase is stable. They concluded that the origin of the stability of the bcc phases comes mainly from the increased entropy due to the low lying $T_1[\xi\xi 2\xi]$ and $T_1[\xi\xi 0]$ phonon branches, as reproduced in Fig. 1 for bcc Ti.

The crystallographic relation in the bcc-to-hcp martensitic transformation was established in 1934 by Burgers [17]:

$$(110)_{\rm bcc}//(0001)_{\rm hcp} \text{ and } [\bar{1}11]_{\rm bcc}//[\bar{2}110]_{\rm hcp}. \quad (1)$$

The transition can be achieved by the superposition of two phonons: i) the zone boundary $[110]T_1$ phonon (we call it T_1N phonon hereafter), and ii) two equivalent long wavelength shears, for instance $(1\bar{1}2)[\bar{1}11]$ and $(\bar{1}12)[1\bar{1}1]$,

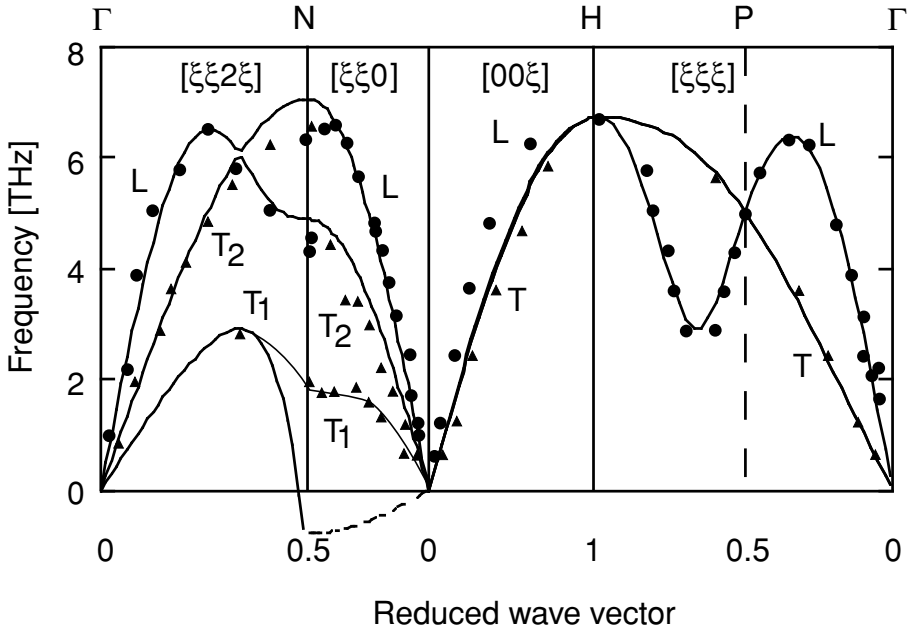

Fig. 1. Phonon dispersions of Ti measured at 1293K by Petry et al. [1]. The fine line shows a Born-von Kármán fit. The curves are calculated using the embedded atom method. The frequency of the N-point phonon of the T_1 branch along the $[\xi\xi 0]$ direction is imaginary due to an unstable potential.

which change the orthogonal lattice with an angle of 109.47° to the hexagonal lattice with 120°. These shears are roughly those given by the initial slope of the transverse $[\xi\xi 2\xi]$ phonon branch with almost $[11\bar{1}]$ polarization. Another martensitic transition of bcc-to-ω can be achieved by a longitudinal phonon of [2/3 2/3 2/3] (we call it ω phonon hereafter).

These three phonons, which achieve the displacements necessary for the two martensitic transitions, lie in the same phonon branch with $[\xi\xi 2\xi]$ propagation and transverse polarization as pointed out by Petry[2]. These are well visualized in Fig. 2. Fig. 2(a) shows the transverse $[\xi\xi 2\xi]$ phonon branch with $[11\bar{1}]$ polarization. The T_1N phonon mode is identical with the transverse phonon in $[\xi\xi 2\xi]$ direction with a (110) polarization and $\xi = 1/2$ as shown in Fig. 2(b). The ω phonon mode is identical with the displacements of the transverse phonon in $[\xi\xi 2\xi]$ direction with $(\bar{1}11)$ polarization and $\xi = 1/3$ as shown in Fig. 2(c).

These phonon-related energies and electronic structures of Zr have been investigated in detail by Ho and co-workers using the first-principles frozen-phonon calculations [4,18,19]. They have shown that the adiabatic potential for the T_1N phonon is unstable with a double-well shape [4], different from the metastable potential for the ω phonon [19]. This gave an impact on the following researches of phenomenological theories or atomistic simulations and brought a notice on the stability of the bcc structure emphasizing the role of

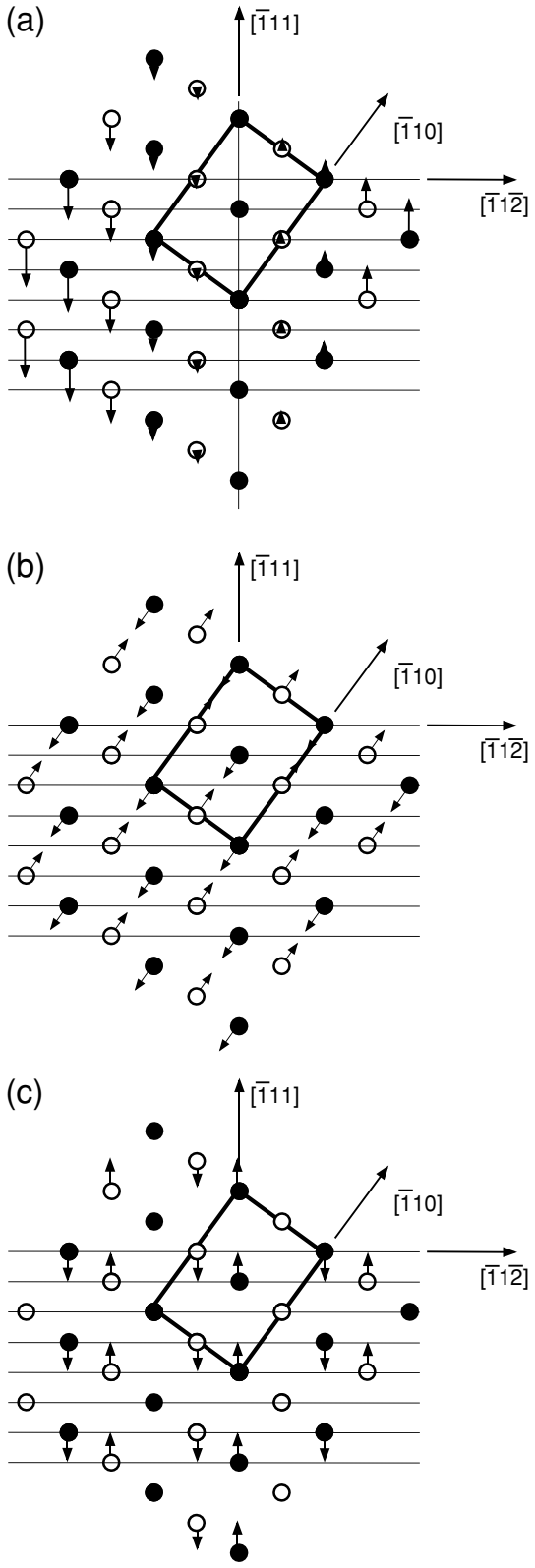

Fig. 2. Displacements of atoms in (110) planes due to (a) the shear of the transverse $[\xi\xi 2\xi]$ phonon branch with $[11\bar{1}]$ polarization, (b) T_1N phonon, and (c) ω phonon. Closed circles: atoms in the (110) plane, open circles: atoms in the (110) planes below and above.

Table 1
Experimental or calculated electronic and vibrational entropies of bcc-hcp transition of Zr and Ti in unit of k_B. The electronic contributions given in parentheses are derived from the other experimental values.

Zr	ΔS_{vib}	ΔS_{band}	ΔS_{tot}
exp.	0.26 [3]	(0.17)	0.40 [20]
calc.	0.126 [7]	0.4 [21]	
	0.143 [5]	0.17 [22]	
Ti	ΔS_{vib}	ΔS_{band}	ΔS_{tot}
exp.	0.29 [1]	(0.13)	0.42 [20]
calc.		0.27 [22]	

the anharmonic effect of the T_1N phonon as shown in Fig.1. In order to obtain the phonon dispersion curves in such unstable potentials, renormalization of the potential or finite-temperature atomistic simulations is necessary.

Willaime and Massobrio [5] derived a simple embedded atom potential for Zr which shows unstable T_1N phonon at the ground state. This anharmonic potential, however, shows a finite frequency at higher temperatures by molecular dynamic simulations. Using the same potential, Salomons [7] calculated the absolute free energies of the hcp and bcc phases as a function of temperature using Monte Carlo simulations with the Einstein-crystal method. The experimental and calculated values of the electronic and vibrational entropies are summarized in Table 1. There is quantitative inconsistency: the vibrational entropies calculated using interatomic potentials show the half of the experimental values. Aside from the inconsistency, the anharmonicity of the T_1N phonon is conceived to play a main role in bcc-hcp transition.

In contrast with the case of Zr, the first principles calculations on Ti are inaccurate, where the ω phase is incorrectly estimated to be more stable than the hcp structure [10,11]. Aside from the accuracy of the ground state calculations, the rough estimations of thermal contributions of electrons and phonons on the bcc-hcp transition have been discussed [22–24]. Atomistic simulation on Ti-V alloys has been made by Crujicic and Dang [25]. Although these researches have shown similar features on bcc-hcp transitions of Ti to those of Zr, it is necessary to investigate the ground state and the thermal effects on electronic structure using accurate first principles calculations.

3 Computational method

Calculations of the electronic structure have been performed using the full-potential linear muffin-tin orbital (FP-LMTO) method [13,14]. The core energy shifts and Perdew and Wang (PW91) type generalized-gradient approximation (GGA) [26] are included. 3s and 3p electrons are treated as "semicore" states so that they are allowed to form narrow bands. Three Hankel tail functions are used. Their decay parameters are chosen $-\kappa^2 = -0.01$Ry (for s, p and d), -1.0Ry (for s, p and d) and -2.0Ry (for s and p). In the calculations, particular care had to be taken for the total energy convergence because of small energy differences between the ω and hcp structures. Very stable convergence was achieved by evaluating the total energy using the Harris-Foulkes [27,28] energy functional of the output and input densities at each iteration. In this connection, we refer the reader to the observation [29,30] that the Harris-Foulkes functional tends to give better energy than that the usual Hohenberg-Kohn-Sham functional would give for an approximate (and nearly self-consistent) "input" density. This property of Harris-Foulkes functional should also be useful in the case where we have undesired small numerical errors in the density. For the calculations at finite electronic temperatures, we replace the band energy part $E_{\rm band}(T=0)$ in the self-consistent total energy at the ground state with the band free energy $F_{\rm band}(T) = E_{\rm band}(T) - TS_{\rm band}$, namely

$$E_{\rm band}(T) = \int \varepsilon n(\varepsilon) f(x) d\varepsilon \tag{2}$$

and

$$S_{\rm band}(T) = k_{\rm B} \int n(\varepsilon)\sigma(x) d\varepsilon, \tag{3}$$

where $f(x) = (1+e^x)^{-1}$ is the Fermi function, $\sigma(x) = -f\ln f - (1-f)\ln(1-f)$ is the entropy function and $x = (\varepsilon - \mu)/(k_{\rm B}T)$ with chemical potential μ. Note that $n(\varepsilon)$ is the density of states at the ground state. Therefore, the free energy at finite temperatures is no longer self-consistent (in the sense of the Kohn-Sham theory at finite temperatures) since the redistribution of the charge density due to the inclusion of thermally excited electronic states is neglected. However, this treatment can be justified to first order because the energy change due to the charge redistribution should be a second order effect.

To describe the bcc to hcp transition, we consider Burgers' distortions. By the following distortions, we obtain the c/a ratio of 1.565[31], which is close to the experimental value of 1.586 for Ti. Keeping the atomic volume constant, the simplest path of transition from a bcc lattice into the hcp structure is through the base-centered orthorhombic structure (oS4 in Pearson's symbol;

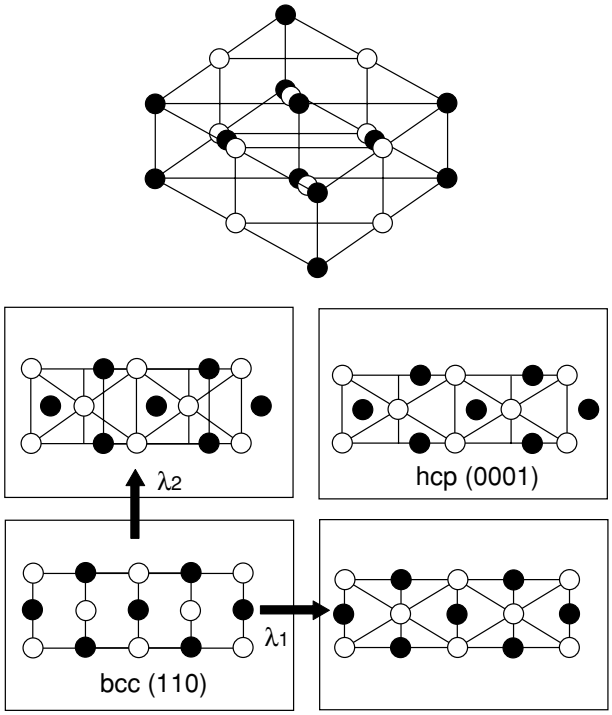

Fig. 3. Transition modes of λ_1 and λ_2 distortions.

space group Cmcm). This includes two independent processes, i.e., a shear deformation from bcc(110) plane to the hexagonal basal plane and an alternate shuffle along $[1\bar{1}0]$ of the planes (T_1N mode in bcc). Intermediate oS4 structures may be mapped on a two-dimensional parameters space, say (λ_1, λ_2), where λ_1 represents the shear deformation and λ_2 represents the shuffle displacement. This is illustrated in Fig. 3. The λ_1 shear is roughly given by the initial slope of the transverse $[\xi\xi 2\xi]$ phonon branch with $[11\bar{1}]$ polarization as shown in Fig. 2(a). The λ_2 shuffling is identical with that shown in Fig. 2(b). The bcc and hcp structures are denoted by (0,0) and (1,1) respectively. Taking the bcc lattice constant a, the orthorhombic lattice parameters are then written as $a_0(\lambda_1) = a/\alpha(\lambda_1)$, $b_0(\lambda_1) = \alpha(\lambda_1)\sqrt{2}a$, and $c_0 = \sqrt{2}a$ with

$$\alpha(\lambda_1) = 1 + \left\{(3/2)^{(1/4)} - 1\right\}\lambda_1. \tag{4}$$

The primitive cell has one of the atoms at

$$\vec{\tau}(\lambda_1, \lambda_2) = \left[0, \frac{3+\lambda_2}{12} b_0(\lambda_1), \frac{1}{4} c_0\right] \tag{5}$$

which derives other atoms by the crystal symmetry.

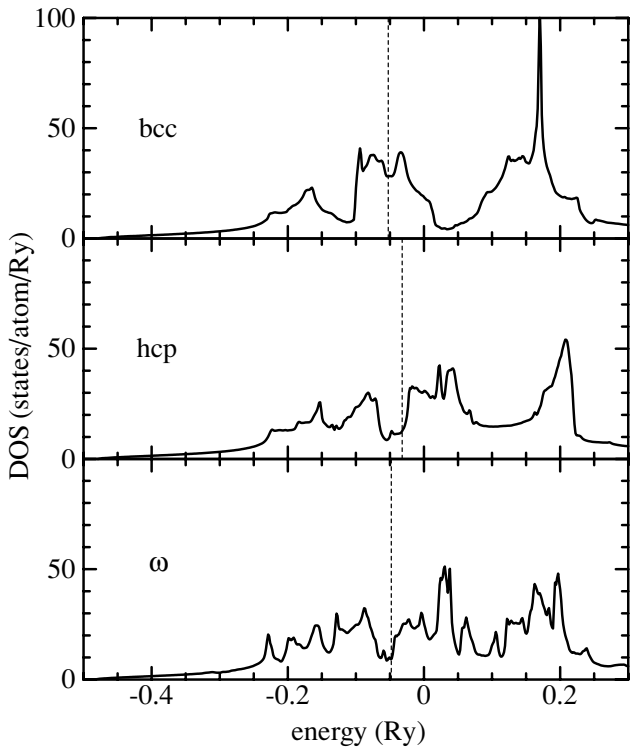

Fig. 4. Electronic density of states at the ground state for the bcc, hcp and ω structures of Ti.

To describe the bcc to ω transition, we consider the displacements shown in Fig. 2(c). The linear parameter λ_3 is taken to be 0 and 1 for bcc and ω structures respectively.

4 Results on the ground state

Since our discussions below rely mainly on the shape of the density of states (DOS) curves, we display our calculated DOS for bcc, hcp and ω structures in Fig. 4. The DOS of bcc is much different from that of hcp. The Fermi level cuts the DOS in the middle of the T_{2g} peak in the bcc structure, whereas it lies in a dip of the DOS for the hcp structure. Those two DOSs are almost identical with those obtained by the previous research [22]. The ω phase shows spiky DOS because of the presence of two sites but the outline is very similar to that of the hcp structure.

The volume dependence of the ground-state energy for hcp, bcc and ω structures of Ti is shown in Fig. 5. The abscissa is the normalized atomic volume Ω/Ω_0, where $\Omega_0 = 119.1$ au^3 is the experimental equilibrium atomic volume of hcp Ti. The c/a ratios of hcp and ω structures are fixed to be the experimental value of 1.586 and an ideal value of $1/\sqrt{8/3}$, respectively. A subtle relative

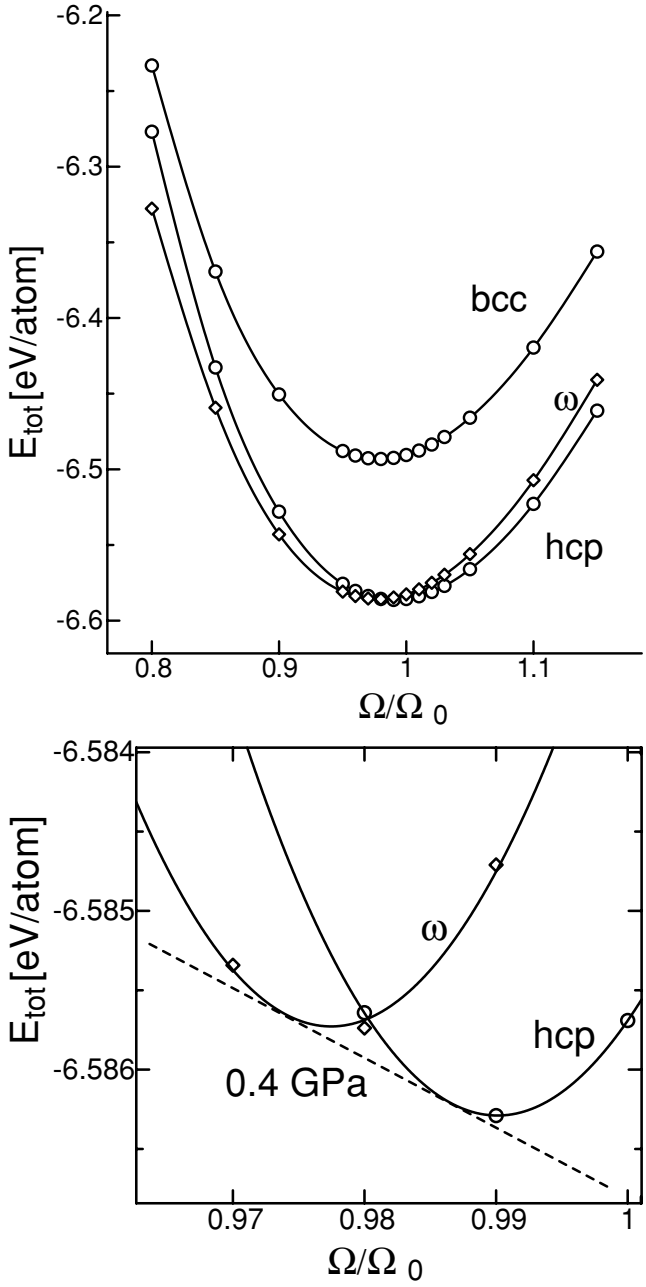

Fig. 5. Volume dependence of the energy at the ground state of Ti for bcc, hcp and ω structures.

stability between the hcp and ω structures is demonstrated in the lower panel of Fig. 5 in an enlarged scale. The calculated values of the equilibrium volume, total energy and bulk modulus are shown in Table 2. Different from the other first principles calculations, hcp structure is correctly estimated to be the most stable structure. From the common tangent for the hcp and ω curves, the transition pressure between them is predicted to be 0.4 GPa, which is comparable to the experimental value of 2 GPa. Those consistent results guarantee that the ground-state calculation for Ti is very accurate.

Table 2
Equilibrium volume, total energy and bulk modulus of bcc, hcp and ω structures.

structure	Ω/Ω_0	$E_{\rm total}$[eV/atom]	B[GPa]
bcc	0.979	-6.4931	107
hcp	0.990	-6.5863	112
ω	0.977	-6.5857	112

Figure 6 shows adiabatic potential-surface for Burgers' path at a fixed atomic volume Ω_0. The bcc structure is located at an unstable saddle point with a strongly negative curvature along the λ_2 displacement. Against the λ_1 shear, the bcc structure is barely stable; the curvature at the minimum is very small. We find that the potential is a double-well against λ_2 for any value of λ_1. For example, at $\lambda_1 = 0$ two minima occur at ± 0.2506 Å with a barrier of 59 meV. This situation is similar to the case of Zr, but the positions of the minima are twice as far and the barrier height is three times larger than those in Zr [4]. Such wider and deeper shape against λ_2 and shallow curve against λ_1 distortions leads to an expectation of larger displacements in Ti than those in Zr. The mean-square displacement estimated from the harmonic approximation with the phonon DOS, however, shows an opposite trend: 0.053 10^{-2}nm^2 for bcc-Ti at 1293K, and 0.06 10^{-2}nm^2 for bcc-Zr at 1188K. We have no guarantee on the application of the harmonic approximation in such an anharmonic system.

The first principles calculations by Ho *et al.* [18] show that in bcc-Zr the valence charge is highly localized along [111] chains under λ_3 distortions, which form linear chains along [111] with very weak interaction between neighboring chains. They pointed out that the ω phonon leaves [111] chains undisturbed, i.e. does not compress or stretch the highly localized d-bonds.

5 Effect of electronic temperature

Temperature dependence of the potential energy against λ_2 distortion is shown in Fig. 7. At the experimental transition temperature of 1155K, the energy difference between the bcc structure and the hcp structure is reduced but shows still a very large value of 80 meV. Along λ_2 distortion the potential shows still clear a double-well shape. The depth of the well decreases with increasing temperature, but is still large at the transition temperature. The thermal excitation is about 100meV at 1155K, which is just above the energy of the bcc structure measured from the hcp. At temperatures higher than 3000K, the bcc structure becomes more stable than hcp, being convex downward at $\lambda_2 = 0$.

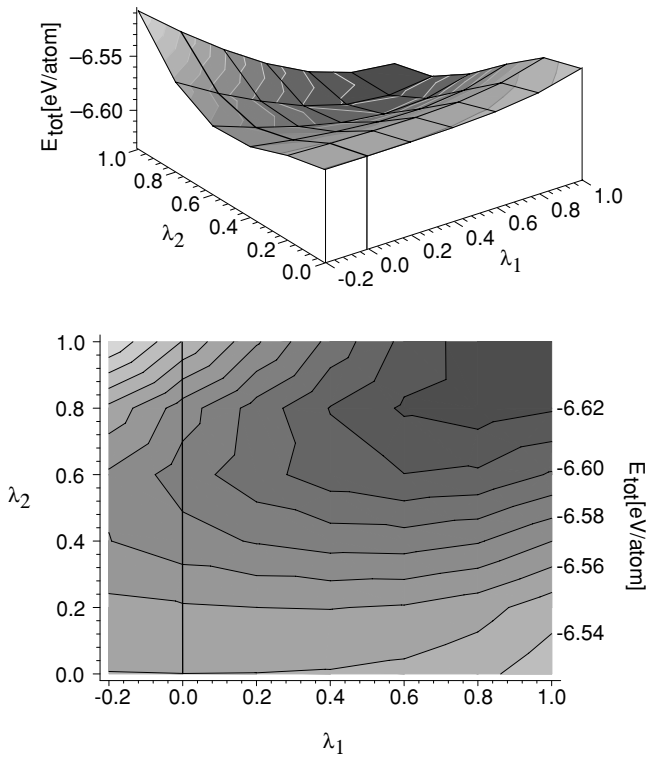

Fig. 6. Adiabatic potential-surface for Burgers' path with contours of step 20 meV. See text for the definitions of λ_1 and λ_2.

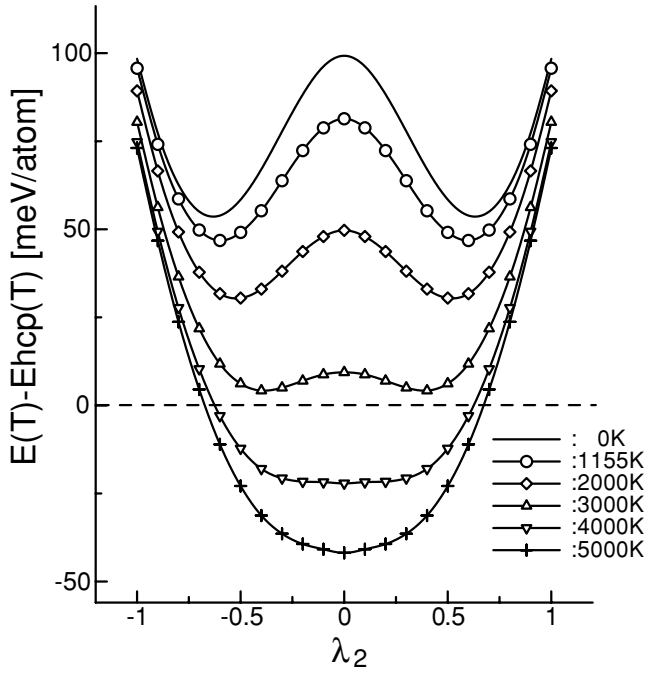

Fig. 7. Temperature dependence of the potential energy at λ_2 distortion.

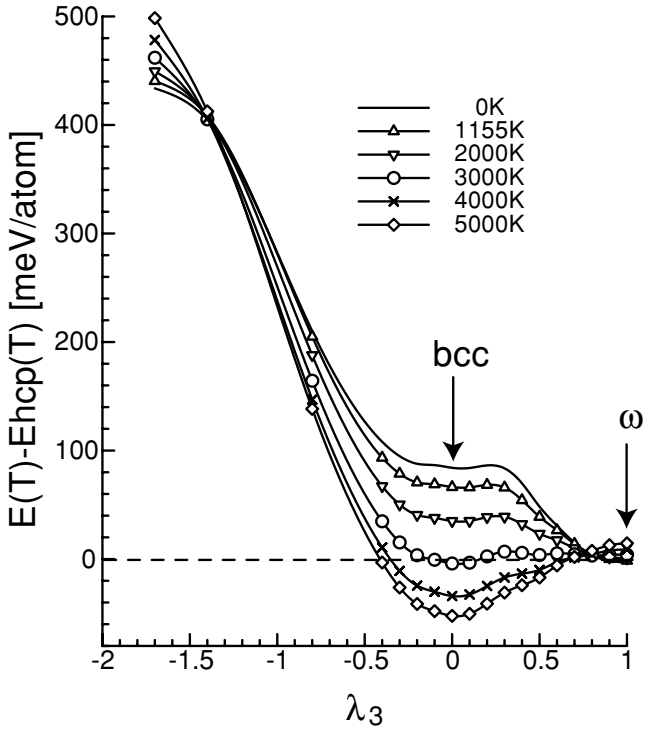

Fig. 8. Temperature dependency of potential at λ_3 distortion.

The temperature dependence of the electronic energy contributions is understood easily from the electronic density of states at the ground state and recalling that the electronic entropy is roughly proportional to the electronic density of state at the Fermi level. As shown in Fig. 4, the bcc structure shows very high density of states in comparison to the hcp structure at the Fermi level. This value decreases the entropy term $-TS_{\rm band}$ faster for the bcc structure than for the hcp with increasing temperature. The thermal electronic contribution obtained by our calculations is close to that obtained by Craievich *et al.* [23]

Temperature dependence of the potential at λ_3 distortion is shown in Fig. 8. At 0K the bcc structure is located at a locally stable but very shallow potential point. The curvature around the bcc structure is much smaller than that of Zr calculated by Chen *et al.* [4] Thus the frequency of the ω phonon mode is much lower than those of Zr. The curvature at the bcc structure is virtually unchanged at the transition temperature. Again as the λ_2 distortion above 3000K the bcc structure is more stable than the hcp and the ω.

The potential surfaces of phonon modes of Ti are not very different from those of Zr. The thermal electronic effects induce little difference from the ground state at the transition temperature, and no drastic change in comparison to Zr. The double-well potential of T_1N phonon, however, is much deeper and wider than that of Zr. The curvature at bcc along ω mode is barely positive. The atomic displacements should show strong anisotropic behavior

and make it difficult to estimate the vibrational entropy. Thus the Gaussian distribution employed by Moroni *et al.* [24] is too simple for Ti. The vibrational contributions on the bcc-hcp transition should be carefully investigated by molecular dynamics using atomistic potentials reproducing the adiabatic potential-surfaces obtained in this research.

6 Conclusions

We performed accurate first principles calculations of Ti and correctly estimated the ground-state structure. The potential surfaces of specific phonon modes related to the structure transitions are qualitatively similar to those of Zr, but quantitatively different: the minima of the double-well potential of the T_1N phonon mode is deeper and wider, and the curvature of the ω phonon mode is extremely small. Those indicate that Ti shows strong anisotropic character of bondings. The thermal electronic contribution leads the bcc structure more stable than the hcp structure above 3000K, but it is very small in magnitude at the transition temperature.

Acknowledgements

MA should like to thank N. M. Duc for useful comments. This work was supported by a Grant-in-Aid for General Scientific Research from the Ministry of Education, Sports, Science, and Culture of Japan, for "Elucidation of the Microscopic Mechanisms of Phase Transitions for Microstructure Control of Materials."

References

[1] W. Petry, A. Heiming, J. Trampenau, M. Alba, C. Herzig, H. R. Schober, G. Vogl, Phys. Rev. B 43 (1991) 10933.

[2] W. Petry, Martensitic Transitions in bcc Metals: Diffusion and Phonons, Technical Report, Institut Laue-Langevin Grenoble (1991).

[3] A. Heiming, W. Petry, J. Trampenau, M. Alba, C. Herzig, H. R. Schober, G. Vogl, Phys. Rev. B 43 (1991) 10948.

[4] Y. Chen, C.-L. Fu, K.-M. Ho, B. N. Harmon, Phys. Rev. B 31 (1985) 6775.

[5] F. Willaime, C. Massobrio, Phys. Rev. Lett. 63 (1989) 2244.

[6] F. Willaime, C. Massobrio, Phys. Rev. B 43 (1991) 11653.

[7] E. Salomons, Phys. Rev. B 43 (1991) 6167.

[8] U. Pinsook, G. J. Ackland, Phys. Rev. B 59 (1999) 13642.

[9] U. Pinsook, G. J. Ackland, Phys. Rev. B 58 (1998) 11252.

[10] R. Ahuja, J. M. Wills, B. Johansson, O. Eriksson, Phys. Rev. B 48 (1993) 16269.

[11] G. Jomard, L. Maguad, A. Pasturel, Phil. Mag., B 77 (1998) 67.

[12] M. Aoki, H. Kawabe, S. R. Nishitani, in preparation.

[13] M. Schilfgaarde, M. Methfessel, The FP program suite, Version 5.4, (1996).

[14] A. T. Paxton, M. Methfessel, H. M. Polatoglou, Phys. Rev. B 41 (1990) 8127.

[15] C. Zener, Phys. Rev. 71 (1947) 846.

[16] J. Friedel, J. Phys. (Paris) 35 (1974) L59.

[17] W. G. Burgers, Physica 1 (1934) 561.

[18] K. M. Ho, C. L. Fu, B. N. Harmon, Phys. Rev. B 28 (1983) 6687.

[19] K.-M. Ho, C. Fu, B. N. Harmon, Phys. Rev. B 29 (1984) 1575.

[20] R. Hultgren, R. D. Desai, D. T. Hawkins, M. Gleiser, K. K. Kelly, D. D. Wagman, Selected Values of the Terhmodynamic Properties of the Elements, Am. Society for Metals, Metals Park, Ohio, 1973.

[21] R. E. Watson, M. Weinert, Phys. Rev. B 30 (1984) 1641.

[22] O. Eriksson, J. M. Wills, D. Wallace, Phys. Rev. B 46 (1992) 5221.

[23] P. J. Craievich, J. M. Sanchez, R. E. Watson, M. Weinert, Phys. Rev. B 55 (1997) 787.

[24] E. G. Moroni, G. Grimvall, T. Jarlborg, Phys. Rev. Lett. 76 (1996) 2758.

[25] M. Crujicic, P. Dang, Mater. Sci. Eng. A 205 (1996) 139.

[26] J. P. Perdew, in: P. Zieshe, H. Eschrig (Eds.), Electronic Structure of Solids 1991, Vol. 11, Akademie Verlag, Berlin, 1991.

[27] J. Harris, Phys. Rev. B 31 (1985) 1770.

[28] W. M. C. Foulkes, R. Haydock, Phys. Rev. B 39 (1989) 12520.

[29] A. J. Read, R. J. Needs, J. Phys: Cond. Mat. 1 (1989) 7565.

[30] M. W. Finnis, J. Phys: Cond. Mat. 2 (1990) 331.

[31] M. Aoki, H. Kawabe, S. R. Nishitani, in: M. Koiwa, K. Otsuka, T. Miyazaki (Eds.), Solid-Solid Phase Transformations, JIMIC-3, The Japan Institute of Metals(Sendai), 1999, pp. 641–644.